ADVANCED ELECTRONIC MATERIALS Open Access
www.advelectronicmat.de

Dielectric-Doped 2D Tellurium Diodes for Zero-Bias Radio Frequency Power Detection

Paula Palacios, Abdelrahman M. Askar, Francisco Pasadas, Mohamed Saeed, Enrique G. Marin, Michael M. Adachi, and Renato Negra*

This work presents a 2D tellurium (Te)-based diode that exploits the doping achieved by atomic layer deposited (ALD) Al_2O_3 to enhance its rectifying performance. The proposed device comprises a Schottky junction that is dielectric-doped to significantly reduce the reverse bias current. A boosted current responsivity four times higher compared to that of undoped devices is achieved, maximizing the performance for radio frequency (RF) power detectors. The application measurement results demonstrate sensitivities as low as −45 dBm, and at −30 dBm RF input power outstanding tangential responsivities up to 6.5 kV W^{-1}, 4.3 kV W^{-1}, and 650 V W^{-1} at 0.5, 1, and 2.5 GHz, respectively, while reaching linear dynamic range (DR) of over 30 dB. These are the highest reported values for 2D-based material devices by almost two orders of magnitude. Furthermore, the DR is ≈10 dB larger compared to state-of-the-art power detectors based on bulk semiconductors.

1. Introduction

2D tellurium (Te) or tellurine has become a promising candidate for the next generation of 2D electronic and optoelectronic devices.[1–3] Naturally p-type, it has hole mobility as high as 700 cm^2 Vs^{-1}, higher than that of transition metal dichalcogenides (TMDs), while being environmentally stable unlike black phosphorous (BP).[1] Yet, due to the novelty of the material, the engineering of tellurene-based devices is still in an early stage and the majority of research has targeted low-frequency p-type transistors or photodiodes.[1] Nevertheless, two different works have shown outstanding performances of 2D Te. First, its application in RF, field-effect transistors (FETs) reaching a cutoff frequency, f_T, and a maximum oscillation frequency, f_{MAX}, of 1.4and 3.6 GHz, respectively.[2] Second, the demonstration of Te-based complementary FETs exhibiting symmetrical performance can be achieved by ALD oxide doping.[3] In this work, both features are combined and exploited in the design of a rectifying diode targeting the implementation of power detectors for RF front-end applications.

The narrow bandgap of multilayer Te[4] is a promising property to implement zero-bias diodes for low-power applications.[5] However, metal-Te Schottky junctions alone might not be sufficient for achieving a performance comparable to that of bulk technologies when used as power detectors. The reason is that the reached asymmetry of the rectifier and, consequently, its responsivity,[5] are limited by the height of the potential barrier formed at the contact. To overcome this effect, this work proposes a Te-based diode that exploits a dielectric doping technique, i.e., the deposition of an oxide on top of the metal-Te contact to alter the barrier height without the need of chemical doping. This way, the dielectric itself is used to modulate the metal and/or Te work functions. To quantitatively evaluate this effect in the rectifying performance, the undoped counterpart is also fabricated and the behavior of both types of devices is compared. The physical modeling of the devices and the achieved measurement results demonstrate that precise engineering of the contact between the metal and the low-dimensional Te is crucial in the achieved rectifying capabilities.

2. Results and Discussion

The two 2D-Te diode architectures studied are presented in **Figure 1**a,b. The first rectifying device, shown in Figure 1c, consists of a Pd-Tellurium-Ti heterostructure, labeled as TM due to the Te-metal Schottky junction formed with the Ti contact.[5] The

P. Palacios, R. Negra
Chair of High Frequency Electronics
RWTH Aachen University
52074 Aachen, Germany
E-mail: paula.palacios@hfe.rwth-aachen.de
A. M. Askar, M. M. Adachi
School of Engineering Science
Simon Fraser University
Burnaby, BC V5A 0A7, Canada
F. Pasadas, E. G. Marin
Departamento de Electrónica y Tecnología de Computadores
Universidad de Granada
Granada 18071, Spain
M. Saeed
InCirT GmbH.
52064 Aachen, Germany

The ORCID identification number(s) for the author(s) of this article can be found under https://doi.org/10.1002/aelm.202400210

DOI: 10.1002/aelm.202400210

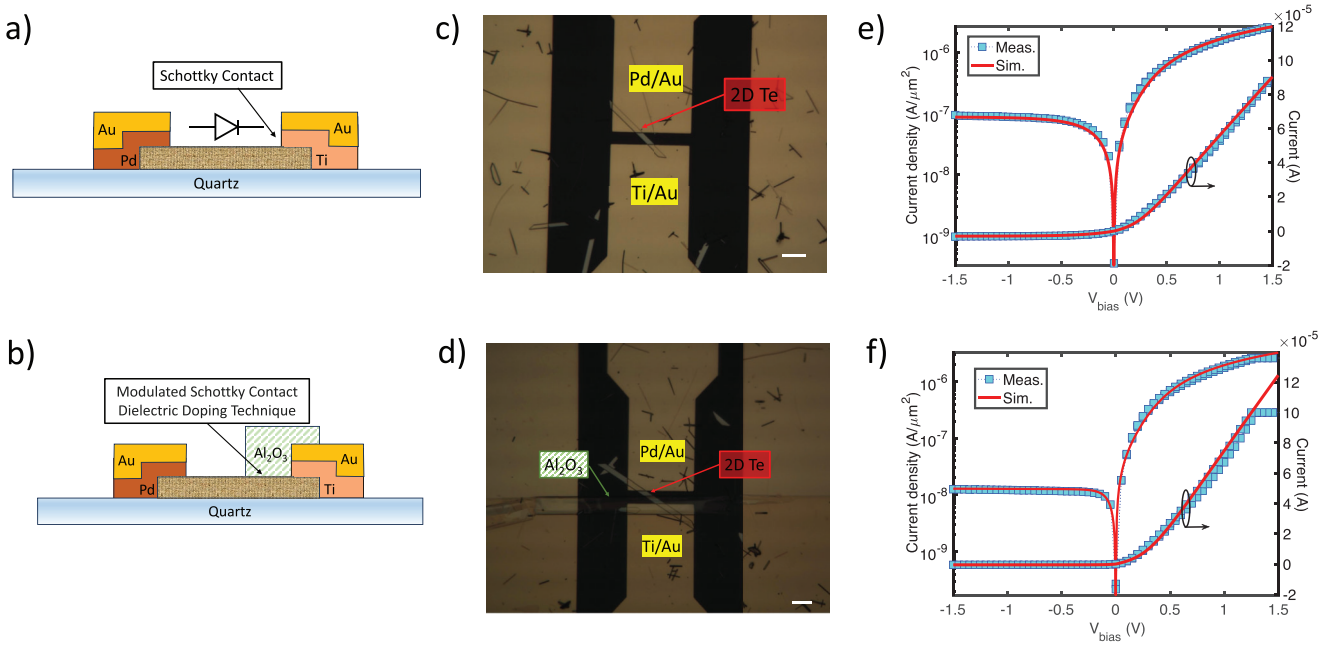

Figure 1. The 2D Te-based RF diodes. a) Cross section of the Schottky Te-metal (TM) device. b) Cross section of the PN-TM device. The ALD oxide placed on top of the Ti-Te contact seeks to alter the Schottky barrier by producing n-type doping. c) Micrograph of the TM diode. An active area for the TM device of 34.7 μm^2 is measured, corresponding to the flake region underneath the Ti electrode. The scale is 13 μm. d) Micrograph of the PN-TM device. Although the Te flake is underneath the metal pads, it can be observed. An active area for the PN-TM device of 106.8 μm^2 is measured, and the scale is 13 μm. e) Predicted (red solid lines) and measured (blue dashed lines) *I*–*V* characteristic curves in linear scale and *J*–*V* in logarithmic scale of the TM diode, and f) PN-TM diode, used to extract the typical detector FOMs. The simulation curves correspond to the obtained results from Equation (6).

second type, fabricated as detailed in the Experimental Section, relies not only on the Te-Ti Schottky barrier but it incorporates an additional ALD dielectric placed around the Schottky junction to explore its impact on the rectifying performance. This technique seeks to produce an n-type doping at the Te-flake, naturally a p-type semiconductor, by inducing the charge transfer from the Al_2O_3.[6] In the literature, dielectric doping has been reported for different 2D materials, including MoS_2,[7] BP,[8] and as previously mentioned, it has already been exploited in Te-based complementary transistors.[3] The micrograph of the device, named for that reason PN-TM diode, is shown in Figure 1d. The measured *I*–*V* and *J*–*V* characteristic curves of the TM and PN-TM diodes are shown in Figure 1e,f, respectively. While in the forward bias region the current increases linearly for both devices, at reverse bias, a clear difference in the magnitude of the reverse current density is observed. In particular, the reverse current density in the case of the PN-TM device is one order of magnitude lower than for the TM counterpart, which straightforwardly impacts on the device asymmetry.

This highly asymmetric behavior of PN-TM technology, crucial for rectifying purposes,[9,10] is additionally verified by the three rectifying figures of merit (FoMs),[11] calculated and plotted in **Figure 2**. While the asymmetry ($f_{ASYM} = |J_{forward}/J_{reverse}|$) increases linearly up to 150 at 1 V in the case of the PN-TM device, it is limited to 10 for the TM device. As previously discussed, this effect is a direct consequence of the dielectric doping technique applied at the Schottky contact surrounding. However, the nonlinearity ($f_{NL} = (dJ/dV)/(J/V)$) is similar for both devices with a maximum limited to 1.7. This is a consequence of the relatively high series resistance, present in both devices. This

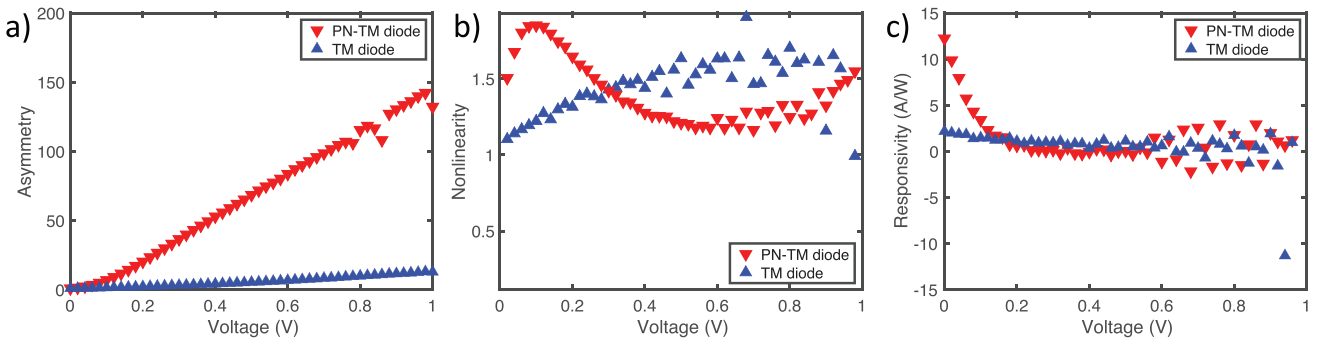

Figure 2. Rectifying figures of merit for TM and PN-TM diodes used as power detectors. a) Asymmetry, b) nonlinearity, and c) responsivity.

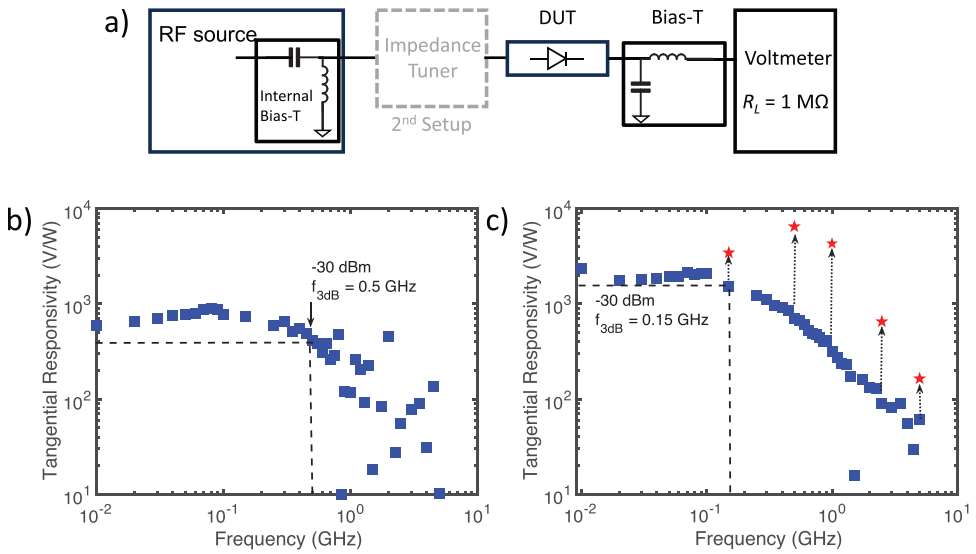

Figure 3. Power detection measurements. a) Power detector test setups. The common blocks for both setups are shown in black, and the added block for the second setup is shown in dashed lines. b) Tangential responsivity results at –30 dBm for the TM diode, and c) for the PN-TM diode. The cuttoff frequency is defined as the frequency where the power drops 3 dB, and corresponds to 0.15 GHz under small-signal conditions as shown in the results without matching (blue square markers). When the impedance tuner is used, the performance improves up to a factor of three (red star markers). The matching is tuned at each frequency.

resistance, partially originated by the contact resistance to the flake, is further studied with the RF characterization and the extracted equivalent circuit as shown in Figures S1 and S2 (Supporting Information). Finally, the third FOM, the current responsivity ($f_{RES} = (d^2J/d^2V)/(2(dJ/dV))$), and a major representative of the expected rectification performance, is calculated. Both devices reach a maximum at 0 V, demonstrating the high potential for zero-bias power detection. However, for the PN-TM diode the obtained value is above 12 A/W, an exceptional result for thin-film technologies,[11] versus the 3 A/W of the TM diode.

Regarding the expected frequency performance, from the RF characterization detailed in the Experimental Section, the cutoff frequency, f_c, defined as the frequency at which the power reaching the junction resistance of the diode is halved, can be estimated at the quiescent point of interest, 0 V, to range between 25 MHz and 0.14 GHz for small-signal applications for the TM diode, and between 4.5 MHz and 0.13 GHz for the PN-TM diode. This approximation is in good agreement with the outcome from power detection measurements without impedance matching, as will be shown.

Based on these results, and the high rectifying potential of the devices, two power detector setups are investigated in this work, as shown in **Figure** 3a. First, the diodes are connected without any input matching to the RF source. At the output, a bias-tee acts as a low-pass filter and drives the rectified current to the voltmeter. This method has been previously used to characterize the extrinsic cutoff frequency of 2D-based diodes.[12] Due to the lack of matching, i.e., the impedance of the diodes is much higher than the 50 Ω of the source, the delivered power to the diode is much less than available from the source. Nevertheless, the tangential responsivity (dV_{out}/dP_{in}) at −30 dBm reaches up to 870 V W^{-1} in the TM diode, while it is higher than 2 kV W^{-1} in the PN-TM device within the bandwidth, as shown in Figure 3b,c, respectively. The corresponding output voltage measurements at −30 and 5 dBm are plotted in **Figure** 4a,b for the TM diode and Figure 4c,d for the PN-TM counterpart, respectively. The measurement results additionally demonstrate the shift of the achieved bandwidth due to the large-signal operation. At −30 dBm (Figure 4a,c), the output voltage shows a decrease factor of 0.7 at 0.5 and 0.15 GHz in the TM and PN-TM diodes, respectively, in better agreement with the calculated f_c. Coherently, this value is maintained at −20 dBm as shown in Figure 4c. However, at 5 dBm (Figure 4b,d), the small-signal assumption does not hold and the diodes are presenting over 0.8 V output DC voltage, which is also changing the quiescent point due to a self-biasing effect. Consequently, at higher powers, f_c increases to 0.85 and 0.7 GHz for TM and PN-TM rectifiers, respectively. Nevertheless, it should be noted that beyond f_c, the responsivities at 1 and 2.5 GHz still reach 316 and 88 V W^{-1} in case of the PN-TM diode, respectively.

The second power detector, including a reactive matching network by an impedance tuner at the input (Figure 3a), is tested on the PN-TM diode only due to the so far demonstrated superior performance. Since the tuner is a narrow band, the matching is only valid at a single frequency, so that the characterization of the rectifying performance at different frequencies implies the optimization of the matching network. Limited by the impedance tuner, the lowest tested frequency is 0.15 GHz. As shown in Figure 3b (Figure 4c for the PN-TM device), the responsivity (output voltage) at –30 dBm, 1 μW input power, improves up to 6.5 kV W^{-1} (6 mV) at 0.5 GHz, which is three (six) times the achieved performance without matching. Furthermore, at 1 and 2.5 GHz up to 4.3 kV W^{-1} (3 mV) and 650 V W^{-1} (1 mV) are demonstrated, respectively. At 5 dBm of input power, the effect of the impedance tuner translates to an exceptional output voltage of 2 V, as shown in Figure 4d. Then, **Figure** 5a,b shows

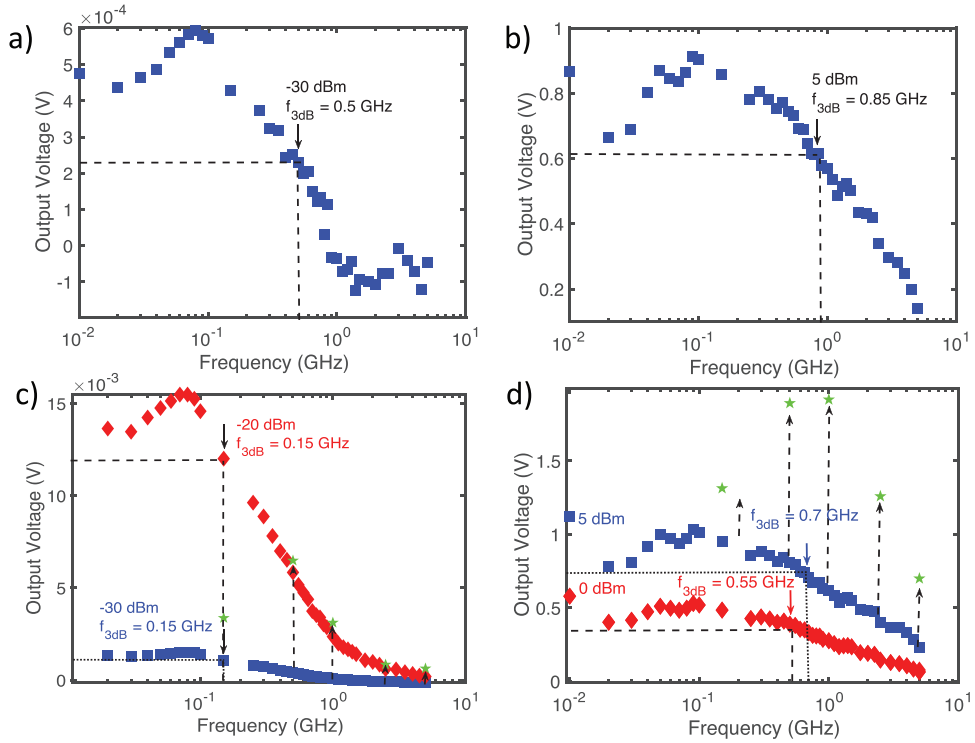

Figure 4. Output voltage over frequency under different input powers. For the TM diode, output voltage at a) –30 dBm and b) 5 dBm. For the PN-TM diode, c) output voltage at –20 and –30 dBm over frequency. At such small input powers, the cutoff frequency remains constant. When the tuner is used at –30 dBm (star markers) the performance improves up to six times depending on the efficiency of the matching. d) Output voltage rectified by PN-TM device at 5 and 0 dBm over frequency. At such higher input powers, the large-signal behavior shifts the cutoff frequency up.[5,13] When the tuner is used at 5 dBm (star markers), the output voltage increases up to a factor of two, i.e., since the quiescent point also shifts due to self-biasing, the responsivity decreases and the improvement factor is less compared to the results at –30 dBm.

the output voltage over input power for both setups, respectively. While the diodes show responsivities in the same order of bulk technologies, within their bandwidth they are also comparable to more complex and active circuits in terms of DR and sensitivities, which are over 30 dB and –45 dBm, respectively.[13] **Table 1** summarizes the performance of different devices based on various materials and their applications. However, it should be highlighted that the measurement setup is critical for the obtained results, and this table merely provides a compact reference to the state-of-the-art. Based on these results, Te shows potential as a power detector. Nevertheless, work is still needed to enable wafer-scale synthesis of the flakes, as well as better control of their size. This is crucial for statistical analysis of the processes and the performance of the device, not carried out in this work precisely for that reason. Furthermore, a better control on the flake can help to reduce the contact resistance, which is the limiting factor in terms of frequency capabilities. An analysis regarding the trade-off between the width of the flake in terms of series

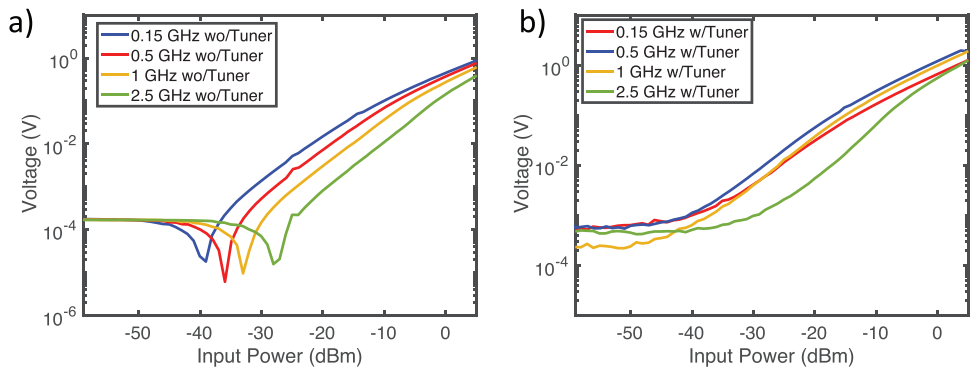

Figure 5. Absolute output voltage over RF input powers for the PN-TM diode in logarithmic scale, when a) there is no matching and b) the impedance tuner is used. The power sensitivity is below –45 dBm while the dynamic range reaches up to 30 dB without matching and slightly decreases when the tuner is used. This is a direct consequence of the self-biasing effect that shifts the quiescent point of the rectifier under higher input powers.

Table 1. Comparison table of 2D diodes and single-device applications.

	Material	Type	f_{RES} [A/W]	Extrinsic f_c [GHz]	Application	Freq. [GHz]	Matching	P_{in} (dBm)	V_{out} (V)	Resp. (V/W)	Sensitivity (dBm)
[14]	WSe_2	Schottky	–	27	Rectifier R_L = 1MΩ	1–10	Resistive	10[b]	0.8/0.6	–	–
[9]	Graphene	MIG	7	–	–	–	–	–	–	–	–
[12]	ZnO	Schottky	–	3.6/5.7	Rectifier R_L = 15MΩ	1/2	No	5	0.2/0.08	–	−10[b]
[11]	CVD Graphene	MIG	13	–	Detector	2.4/49.4	Resistive	4.77	0.462/0.456	2.8/1.1	–
[15]	MoS_2	Schottky	5	10	E. Harvester R_L = 10kΩ	0.1–10	No	5	3V@2.4GHz 1.5@10GHz	–	−20[b]
This work	Te	Schottky	3	0.14[a]	Detector R_L = 1MΩ	0.15/0.5/1/2.4	No	5	0.85/0.74/0.56/0.33	744/416/117/55	−45
This work	Te	Doped Schottky	12	0.13[a]	Detector R_L = 1MΩ	0.15/0.5/1/2.4	No/Reactive	5	0.95;0.8;0.6;0.4/1.3;1.89;1.9;1.2	1535;665;316;88/3.5k;6.5k;4.3k;640	−45

[a] Upper limit under small signal conditions. [b] Obtained as the minimum power of the shown plots of the measurements.

resistance reduction and increase of the junction capacitance is still needed.

Finally, to provide further insights about the electrical performance of the TM and PN-TM heterostructures, a theoretical physics-based model to qualitatively interpret the transport of both devices is developed. The predicted *I*–*V* and *J*–*V* curves are also depicted in Figures 1e,f (red solid lines) showing an outstanding agreement with the experimental measurements for both devices. First, the physical principles defining the operation of the TM rectifier are presented, then the resulting change in the device behavior due to the presence of the Al_2O_3 layer in the rectifying contact is discussed.

According to the experimental and computational evaluations of Pd and Te work functions, the Pd-Te junction is assumed to form an ohmic contact.[16] In particular, the considered work function of Pd, $\phi_{Pd} = 5.67$ eV,[17] is significantly larger than the Te electron affinity, $\chi_{Te} = 4.3$ eV,[18] and their contact forms a dipole layer (contact gap) at the Pd-Te interface, which produces a charge transference that keeps the Fermi energies aligned and results in a highly p-doped Te. The electrostatics of the Pd-Te contact are described by:

$$\phi_{Pd} - \chi_{Te} - \frac{E_{g,Te}}{2q} - V_{ch} = \frac{Q_{Te}(V_{ch}) + Q_{res}}{C_{gap,Pd-Te}} \quad (1)$$

where the Te work function is $\phi_{Te} = \chi_{Te} + \frac{E_{g,Te}}{2q} + V_{ch}$, with $\chi_{Te} = 4.3$ eV and $E_{g,Te} = 0.38$ eV,[19] the electron affinity and bandgap. Additionally, $V_{ch} = -(E_F - E_i)/q$, with E_F the Fermi level, E_i the intrinsic energy, and q the elementary charge. $C_{gap,Pd}$ is the capacitive coupling originated at the contact gap, $Q_{res} = -35\,\mathrm{mCm^{-2}}$ is the residual charge density due to additional fixed charge that owes to impurities or uncontrolled doping, and $Q_{Te}(V_{ch})$ is the net charge density in the Te-channel, which is calculated assuming the effective mass approximation and employing Fermi–Dirac statistics at the conduction and valence bands:[5,20]

$$Q_{net}(V_{ch}) = qV_tC_{dq,p}\log\left(1 + e^{\frac{V_{ch} - \frac{E_{g,Te}}{2q}}{V_t}}\right) - qV_tC_{dq,n}\log\left(1 + e^{-\frac{V_{ch} + \frac{E_{g,Te}}{2q}}{V_t}}\right) \quad (2)$$

Here $V_t = k_BT/q = 25.4$ meV is the thermal voltage, with k_B the Boltzmann constant, $T = 300$ K the temperature, and $C_{dq,n} = q^2D_{0,n}$ ($C_{dq,p} = q^2D_{0,p}$) is the degenerated-quantum capacitance for electrons (holes), representing upper-limit values under heavy degeneration densities.[21] There,

$$D_{0,n} = g_{e,1}(m^*_{e,1}/2\pi\hbar^2) \quad (3)$$

and

$$D_{0,p} = g_{h,1}(m^*_{h,1}/2\pi\hbar^2) + g_{h,2}(m^*_{h,2}/2\pi\hbar^2)\exp[-\Delta E_{h,1\to2}/k_BT] \quad (4)$$

are the effective density of states at the edge of the conduction and valence bands respectively, with $\hbar$ standing for the reduced Planck constant. The terms $g_{e,1} = 4$, $g_{h,1} = 2$, $g_{h,2} = 2$ are the degeneracy factors, and $m^*_{e,1} = 0.085m_e$, $m^*_{h,1} = 0.5m_e$, $m^*_{h,2} = 0.1m_e$,[18,22–28] the conduction band and valence band effective masses at the first and second valleys, respectively, in the vicinity of the symmetry H-point in the case of Tellurium,[22,29]

with m_e the electron rest mass. The significance of the valence band second valley is notable due to the energy proximity between valleys, $\Delta E_{h,\,1\to2} = 0.15$ eV,[24,25] just few $k_B T$[30,31] at room temperature. However, in the conduction band, the second valley is significantly distant in energy ($\Delta E_{e,\,1\to2} = 1.12$ eV) and can be disregarded for practical purposes.[24] Solving Equation (1) for the TM device, results in $V_{ch} = 0.32$ eV, meaning that the p-type Te is degenerated ($V_{ch} > E_{g,\,Te}/2$). Additionally, the ohmic contact between the Pd and Te is confirmed as $\phi_{Pd} > \phi_{Te}$.

On the other hand, when analyzing the rectifying metal-semiconducting (MS) Ti-Te contact, the Te-flake thickness $t_{Te} \sim 160$ nm results in the formation of a depletion layer between the interface of the Ti metal and the neutral Te flake region underneath. Consequently, a built-in potential (ϕ_{bi}) is formed with a corresponding Te depletion-layer thickness (W_{dep}). Thus, the electrostatics of the MS Ti-Te contact can be understood by solving the potential loop at such interface:

$$\phi_{Ti} - \chi_{Te} - \frac{E_{g,Te}}{2q} - V_{ch} + \phi_{bi} = \frac{Q_{Te}(V_{ch} - \phi_{bi})}{C_{gap,Ti-Te}} \tag{5}$$

with $\phi_{Ti} = 4.327$ eV. The current density through the MS junction is then attributed to the thermionic emission of carriers above the barrier materials[5] as:

$$J_{th} = q\frac{C_{dq}V_t^2}{2\pi\hbar}e^{-\frac{\phi_b}{V_t}}\left(e^{\frac{V_{bias}}{\eta V_t}} - 1\right) \tag{6}$$

where ϕ_b is the Schottky barrier height (SBH); η is the ideality factor; and $C_{dq} = \sqrt{C_{dq,n}C_{dq,p}}$. In the case of the TM-device, ϕ_{bi} varies (with bias) from 0.4 to 0.26 eV, as can be observed in Figure S3 (Supporting Information) (red solid line). Hence, the corresponding variation of the depletion-layer thickness, $W_{dep} = \sqrt{2q\epsilon_{Te}\phi_{bi}t_{Te}/\left(Q_{Te}(V_{ch})\right)}$, ranges from 25 nm to 30.8 nm within the voltage window from –1.5 and 1.5 V. These results confirm the partial charge depletion in the Te: $W_{dep} < t_{Te}$. Figure S3 (Supporting Information) also shows the potential energy $V_{ch} - \phi_{bi}$ (blue solid line) ranging from –85 to 53 meV, i.e. the Te Fermi level at the Ti-Te interface is located within the bandgap (i.e., within $\pm E_{g,\,Te}/2$), bringing to light that a depletion layer appears at the Te-channel close to the Ti-Te interface. The rectifying contact is also confirmed with $\phi_{Ti} < \phi_{Te}$. Thus, the transport properties of the Schottky contact are strongly dependent on the shape of the potential energy barrier and several physical effects can alter this shape, being an image barrier lowering the most impacting. This effect is estimated here according to the model proposed by some of the authors in Refs. [5, 32] and results in a Schottky barrier lowering (SBL) ranging from 29.5 to 26.8 meV within the considered bias window. Figure S3 (Supporting Information) also shows the bias-dependent barrier, ϕ_b, behavior (black solid line). In particular, for $V_{bias} < 0$ the barrier from the metal to the Te channel dominates, $\phi_{b,\,m} = \chi_{Te} + E_{g,\,Te} - \phi_{Ti} - \text{SBL}$. Except for the slight effect of the SBL, $\phi_{b,\,m}$ is fixed, as it is observed in the bias dependence of the reverse current density in Figure 1e. However, for $V_{bias} > 0$, the barrier seen from the Te channel to the Ti metal dominates, $\phi_{b,\,Te} = \phi_{bi}$, which is highly bias-tunable (black solid line in Figure S3, Supporting Information), causing a large modulation in the forward current (Figure 1e).

In regard to the PN-TM device, although the same theoretical framework holds, adjustments of the parameters affected by the charge transfer from the Al_2O_3 are required. These are: 1) the residual charge density, $Q_{res,\,PN} = -42\text{mCm}^{-2}$, corresponding to a effective n-type doping of the Te flake $n_{Al_2O_3} = 2.62 \times 10^{13}\text{cm}^{-2}$, and 2) the Ti work function which is slightly reduced by $\Delta\phi_{Ti} = 77$meV, *i.e.* $\phi_{Ti,\,PN} = \phi_{Ti} - \Delta\phi_{Ti} = 4.25$eV. The latter effect meaning that the ALD Al_2O_3 on top of the metal electrode can lower its work function by inducing surface dipole formation, facilitating charge transfer, causing band bending, and passivizing surface states, which collectively reduces the energy required to remove electrons from the surface. These two combined effects ultimately increases the Schottky barrier at reverse bias $\phi_{b,\,m,\,PN\text{-}TM} = \chi_{Te} + E_{g,\,Te} - \phi_{Ti,\,PN} - \text{SBL}$. Therefore, this behavior of the barrier that can be controlled by the doping oxide is responsible of the rectifying performance enhancement in terms of asymmetry and responsivity that has been empirically demonstrated.

This work presents a 2D-Te-based diode specifically engineered for power detection in low-power front-ends. The device exploits the observed impact of the Te-flake doping on the rectification performance. Compared to the device without dielectric doping technique, the power detector performance is improved over a factor of two. Furthermore, in particular, for the PN-TM diode, the measured responsivities are comparable to the reported in conventional bulk semiconductors while having a significantly larger dynamic range. Meanwhile, compared to other and more mature 2D materials, the responsivity is almost two orders of magnitude higher within the device bandwidths.[10,11,33] The presented results show an excellent performance up to the UHF band, which embraces current RFID and Bluetooth among multiple other communication standards. This device demonstrates the potential and versatility of 2D-Te, and paves the way for next generation thin-film RF detectors and rectifiers based on this material.

3. Experimental Section

PN-TM Device Fabrication: Initially, the 2D Te flakes were prepared following a standard hydrothermal synthesis procedure. First, 0.04895 g of Na_2TeO_3 and 0.236 g of PVP-55K were added to 16.5 mL of de-ionized (DI) water under magnetic stirring to form a homogeneous solution. Next, 1.66 mL of aqueous ammonia (25% wt/wt%) was added followed by 0.84 mL of hydrazine hydrate (85% wt/wt%). The mixture was sealed in a 50 mL Teflon-lined stainless steel autoclave and heated at 180 °C for 20 h before naturally cooling it down to room temperature. For purification, the obtained silver-grey product was washed several times by centrifuging at 5000 rpm for 5 min to remove the remaining PVP. After washing and purification, the Te flakes were redispersed in DI water. The estimated achieved thickness of the flakes was between ≈120 and ≈160 nm. Optical images of other flakes were used to estimate this range by comparing the appearance of the flake in the device to other flakes for which thickness was measured by AFM technique.

Then, the PN device fabrication started with drop-casting the 2D Te containing DI water solution on the pre-cleaned quartz substrates (≈2 cm x 2 cm) and letting it dry. The samples were annealed for 5 min at 90 °C and after they cooled down they were cleaned further by having them 5 min in Acetone followed by another 5 min in IPA to then get dried with N2. Using optical maskless lithography (laser writer) a suitable 2D Te flake was chosen, and the first contact was patterned and later deposited using e-beam evaporation of 10 nm (with very slow deposition rate, 0.2° A s^{-1}) followed by 150 nm Au. Titanium was chosen due to its similar work function with the Te flake to form the rectifying Schottky contact.[3] The first contact

fabrication ended with lift-off process. Next, the local Al_2O_3 was deposited by ALD after patterning an opening with a laser writer. This partially exposed the part of the 2D Te flake contacted by the first Ti/Au contact, while leaving about half of the flake unexposed during the ALD process, to be later contacted with the ohmic second contact (Pd/Au). The ALD process was carefully designed following directions from earlier studies that reported similar n-type doping of other 2D materials through Al_2O_3 ALD process. H_2O-based deposition using trimethylaluminum (TMA) as the precursor was adopted, with 300 cycles to achieve a thickness of ≈27 nm. Standard Al_2O_3 ALD processes were usually done at 250 °C, but deposition temperature of 100 °C was used instead to avoid degradation of the 2D Te flake quality observed at higher processing temperature and associated challenges reported in the literature.[34] At the end of the deposition, lift-off process was used to complete the local deposition of Al_2O_3. Studying the effect of the Al_2O_3 ALD deposition temperature and thickness on the rectifying behavior of the PN-TM diode was beyond the scope of this study and could be carried in a future work. Then, the Pd/Au contact (10 nm/150 nm) was patterned (like the first contact) on the 2D Te part of the flake with no Al_2O_3 deposited, and a lift-off process followed which completed the fabrication of the device. The use of Pd, which possessed a large work function, was preferred as ohmic contact with the 2D Te flake showing a lower contact resistance.[3] It is important to highlight that device contacts were patterned in such a way to make current flow along the [0001] direction, reported earlier in the literature to have higher mobility (1.5× more) than the other [1210] direction.[1]

RF Characterization and Equivalent Circuit Extraction: The RF characterization was carried out by means of *S*-parameter measurements from 10 MHz to 67 GHz at different bias points between −1 and 1 V. From these results, an equivalent small-signal circuit was extracted for the TM and PN-TM diodes at the quiescent point of interest, 0 V, as shown in Figures S1 and S2 (Supporting Information), respectively. The devices presented a more complex behavior compared to a typical single Schottky contact equivalent circuit. The calculation of the value of the extracted elements, and the choice of the topology were carried out as pointed out in Ref. [5]. Likewise, the same procedure as in Ref. [5] was employed to calculate the f_c range.

Supporting Information

Supporting Information is available from the Wiley Online Library or from the author.

Acknowledgements

P.P., A.A., and F.P. contributed equally to this work. The authors thank the German Research Foundation (DFG) under the projects GLECS2 (No. 653408), MOSTFLEX (653414), the Natural Sciences and Engineering Research Council of Canada (NSERC) (RGPIN-2017-05810 and ALLRP 577611-22), and the European Commission under the Horizon 2020 projects Graphene Flagship (No. 785219 and 881603). This work is part of the research projects TED2021-129938B-I00 FlexPowHar and CNS2023-143727 RECAMBIO both funded by MCIN/AEI/10.13039/501100-011033 and the European Union NextGenerationEU/PRTR. This work is also funded by the R+D+i project A-ING-253-UGR23 AMBITIONS co-financed by Consejería de Universidad, Investigación e Innovación and the European Union under the FEDER Andalucía 2021-2027. A.M.A. is supported by a Vanier Canada Graduate Scholarship. The authors would like to acknowledge CMC Microsystems for the provision of products and services that facilitated this research. This work made use of the 4DLABS shared facilities supported by the Canada Foundation for Innovation (CFI), British Columbia Knowledge Development Fund (BCKDF), and Western Economic Diversification Canada (WD). This work was further supported by Simon Fraser University.

Conflict of Interest

The authors declare no conflict of interest.

Data Availability Statement

The data that support the findings of this study are available from the corresponding author upon reasonable request.

Keywords

2D, diode, dielectric, doping, power detection, RF, Tellurium

Received: March 12, 2024
Revised: May 20, 2024
Published online:

[1] Y. Wang, G. Qiu, R. Wang, S. Huang, Q. Wang, Y. Liu, Y. Du, W. A. Goddard III, M. J. Kim, X. Xu, P. D. Ye, W. Wu, *Nat. Electron.* **2018**, *1*, 228.
[2] K. Xiong, G. Qiu, Y. Wang, L. Li, A. Göritz, M. Lisker, M. Wietstruck, M. Kaynak, W. Wu, D. Y. Peide, A. Madjar, J. C. M. Hwang, In,*2021 IEEE MTT-S Int. Microwave Symp. (IMS)*, IEEE, New Jersey, **2021**, pp. 319–322.
[3] G. Qiu, M. Si, Y. Wang, X. Lyu, W. Wu, P. D. Ye, In *2018 76th Device Research Conference (DRC)*. Institute of Electrical and Electronics Engineering Inc., Santa Barabara, August, **2018**, pp. 1–2.
[4] G. Qiu, A. Charnas, C. Niu, Y. Wang, W. Wu, P. D. Ye, *npj 2D Mater. Appl.* **2022**, *6*, 17.
[5] A. M. Askar, P. Palacios, F. Pasadas, M. Saeed, M. R. Mohammadzadeh, R. Negra, M. M. Adachi, *npj 2D Mater. Appl.* **2023**, *7*, 70.
[6] A. Piacentini, D. Marian, D. S. Schneider, E. González Marín, Z. Wang, M. Otto, B. Canto, A. Radenovic, A. Kis, G. Fiori, M. C. Lemme, D. Neumaier, *Adv. Electron. Mater.* **2022**, *8*, 2200123.
[7] A. Valsaraj, J. Chang, A. Rai, L. F. Register, S. K. Banerjee, *2D Mater.* **2015**, *2*, 045009.
[8] H. Mu, W. Yu, J. Yuan, S. Lin, G. Zhang, *Mater. Futures* **2022**, *1*, 012301.
[9] R. Urcuyo, D. L. Duong, H. Y. Jeong, M. Burghard, K. Kern, *Adv. Electron. Mater.* **2016**, *2*, 1600223.
[10] M. Saeed, P. Palacios, M.-D. Wei, E. Baskent, C.-Y. Fan, B. Uzlu, K.-T. Wang, A. Hemmetter, Z. Wang, D. Neumaier, M. C. Lemme, R. Negra, *Adv. Mater.* **2022**, *34*, 2108473.
[11] M. Shaygan, Z. Wang, M. S. Elsayed, M. Otto, G. Iannaccone, A. H. Ghareeb, G. Fiori, R. Negra, D. Neumaier, *Nanoscale* **2017**, *9*, 11944.
[12] D. G. Georgiadou, J. Semple, A. A. Sagade, H. Forstén, P. Rantakari, Y.-H. Lin, F. Alkhalil, A. Seitkhan, K. Loganathan, H. Faber, T. D. Anthopoulos, *Nat. Electron.* **2020**, *3*, 718.
[13] E. Reato, P. Palacios, B. Uzlu, M. Saeed, A. Grundmann, Z. Wang, D. S. Schneider, Z. Wang, M. Heuken, H. Kalisch, A. Vescan, A. Radenovic, A. Kis, D. Neumaier, R. Negra, M. C. Lemme, *Adv. Mat.* **2022**, *34*, 2108469.
[14] S. J. Yang, K.-T. Park, J. Im, S. Hong, Y. Lee, B.-W. Min, K. Kim, S. Im, *Nat. Commun.* **2020**, *11*, 1574.
[15] X. Zhang, J. Grajal, J. L. Vazquez-Roy, U. Radhakrishna, X. Wang, W. Chern, L. Zhou, Y. Lin, P.-C. Shen, X. Ji, X. Ling, A. Zubair, Y. Zhang, H. Wang, M. Dubey, J. Kong, M. Dresselhaus, T. Palacios, *Nature* **2019**, *566*, 368.
[16] O. Olawole, D. De, O. Olawole, R. Lamba, E. Joel, S. Oyedepo, A. Ajayi, O. Adegbite, F. Ezema, S. Naghdi, T. Olawole, O. Obembe, K. Oguniran, *Heliyon* **2022**, *8*, e11030.
[17] F. A. Chaves, D. Jiménez, A. A. Sagade, W. Kim, J. Riikonen, H. Lipsanen, D. Neumaier, *2D Mater.* **2015**, *2*, 025006.
[18] M. Jałochowski, P. Mikołajczak, M. Subotowicz, *Phys. Status Solidi A* **1972**, *14*, K135.
[19] S. Arora, Y. K. Vijay, *AIP Conf. Proc.* **2018**, *1953*, 030083.

[20] F. Pasadas, E. G. Marin, A. Toral, F. G. Ruiz, A. Godoy, S. Park, D. Akinwande, D. Jiménez, *npj 2D Mater. Appl.* **2019**, *3*, 1.
[21] N. Ma, D. Jena, *2D Mater.* **2015**, *2*, 015003.
[22] C. Şahin, J. Rou, J. Ma, D. A. Pesin, *Phys. Rev. B* **2018**, *97*, 205206.
[23] D. K. Sang, B. Wen, S. Gao, Y. Zeng, F. Meng, Z. Guo, H. Zhang, *Nanomaterials* **2019**, *9*, 1075.
[24] J. Qiao, Y. Pan, F. Yang, C. Wang, Y. Chai, W. Ji, *Sci. Bull.* **2018**, *63*, 159.
[25] V. Anzin, M. Eremets, Y. V. Kosichkin, A. Nadezhdinskii, A. Shirokov, *Phys. Status Solidi A* **1977**, *42*, 385.
[26] D.-Q. Yang, L.-Q. Zhu, J.-L. Wang, W. Xia, J.-Z. Zhang, K. Jiang, L.-Y. Shang, Y.-W. Li, Z.-G. Hu, *Phys. Status Solidi (b)* **2022**, *259*, 2100625.
[27] H. Shinno, R. Yoshizaki, S. Tanaka, T. Doi, H. Kamimura, *J. Phys. Soc. Jpn.* **1973**, *35*, 525.
[28] D. Thanh, *Solid State Commun.* **1971**, *9*, 631.
[29] R. Enderlein, A. Hache, *Phys. Status Solidi (b)* **1973**, *60*, 739.
[30] A. Kormányos, G. Burkard, M. Gmitra, J. Fabian, V. Zólyomi, N. D. Drummond, V. Fal'ko, *2D Mater.* **2015**, *2*, 022001.
[31] F. A. Rasmussen, K. S. Thygesen, *J. Phys. Chem. C* **2015**, *119*, 13169.
[32] F. Pasadas, M. Saeed, A. Hamed, Z. Wang, R. Negra, D. Neumaier, D. Jiménez, *IEEE Electron Device Lett.* **2019**, *40*, 1005.
[33] M. Saeed, A. Hamed, Z. Wang, M. Shaygan, D. Neumaier, R. Negra, *IEEE Trans. Microwave Theory Tech.* **2018**, *66*, 4.
[34] D. Y. Park, H. M. Yu, B. G. Jeong, S.-J. An, S. H. Kim, M. S. Jeong, *Nanomaterials* **2021**, *11*, 2735.